The Photobleaching Sequence of a Short-Wavelength Visual Pigment†

Anakarin Kusnetzow,‡,§,|| Abhiram Dukkipati,§ Kunnel R. Babu,⊥ Deepak Singh,§ Bryan W. Vought,§,@ Barry E. Knox,*,⊥ and Robert R. Birge*,‡,§

Departments of Chemistry and of Molecular and Cell Biology, University of Connecticut, 55 North Eagleville Road, Storrs, Connecticut 06268-3060, Departments of Chemistry and Biology, Syracuse University, 111 College Place, Syracuse, New York 13244-4100, and Department of Biochemistry and Molecular Biology, State University of New York Upstate Medical University, 750 East Adams Street, Syracuse, New York 13210

Received February 23, 2001; Revised Manuscript Received April 27, 2001

ABSTRACT: The photobleaching pathway of a short-wavelength cone opsin purified in delipidated form (λ_{max} = 425 nm) is reported. The *batho* intermediate of the violet cone opsin generated at 45 K has an absorption maximum at 450 nm. The *batho* intermediate thermally decays to the *lumi* intermediate (λ_{max} = 435 nm) at 200 K. The *lumi* intermediate decays to the *meta I* (λ_{max} = 420 nm) and *meta II* (λ_{max} = 388 nm) intermediates at 258 and 263 K, respectively. The *meta II* intermediate decays to free retinal and opsin at >270 K. At 45, 75, and 140 K, the photochemical excitation of the violet cone opsin at 425 nm generates the *batho* intermediate at high concentrations under moderate illumination. The *batho* intermediate spectra, generated via decomposing the photostationary state spectra at 45 and 140 K, are identical and have properties typical of *batho* intermediates of other visual pigments. Extended illumination of the violet cone opsin at 75 K, however, generates a red-shifted photostationary state (relative to both the dark and the *batho* intermediates) that has as absorption maximum at ∼470 nm, and thermally reverts to form the normal *batho* intermediate when warmed to 140 K. We conclude that this red-shifted photostationary state is a metastable state, characterized by a higher-energy protein conformation that allows relaxation of the all-*trans* chromophore into a more planar conformation. FTIR spectroscopy of violet cone opsin indicates conclusively that the chromophore is protonated. A similar transformation of the rhodopsin binding site generates a model for the VCOP binding site that predicts roughly 75% of the observed blue shift of the violet cone pigment relative to rhodopsin. MNDO-PSDCI calculations indicate that secondary interactions involving the binding site residues are as important as the first-order chromophore protein interactions in mediating the wavelength maximum.

Two types of photoreceptor cells, rods and cones, mediate vision in vertebrates. Rods are responsible for scotopic (low-light) vision, and cones are responsible for color discrimination and high-flux visual acuity (*1*−*3*). The visual opsins contain an 11-*cis*-retinal chromophore covalently bound to the apoprotein via a Schiff base linkage to a conserved lysine residue (*4*). The 11-*cis* chromophore isomerizes to an all-*trans* conformation upon light activation, which induces the sequential formation of a series of thermal intermediates (*5*, *6*). The key biological state, the *meta II*[1] intermediate, activates the G-protein transducin, which in turn initiates the visual cascade (*7*, *8*). The vertebrate visual pigments are classified into five groups based on sequence similarity (*9*−*12*) as shown in the dendogram of Figure 1 based on the review by Ebrey and Koutalos (*13*). We have updated the absorption maxima for the SWS1 pigment group using data from refs *14*−*20*. It should be noted that some of the absorption maxima listed in Figure 1 were assigned from very small pigment samples and are subject to uncertainty. The pigments responsible for scotopic vision (rhodopsins or RH1) absorb maximally at ∼500 nm. The pigments that mediate photopic vision are subdivided into middle- to long-wavelength (M/LWS, >510 nm), two short-wavelength (SWS2, 440−460 nm, and SWS1, 350−450 nm), and rhodopsin-like, middle-wavelength (RH2, 460−510 nm) groups. The absorption maxima of the majority of the pigments in each group fall within a constrained spectral range, suggesting that the spectral tuning mechanism is mediated by the protein binding site (*9*−*12*). The photobleaching kinetics of rod and cone opsins may play an

† This work was supported in part by NIH Grants GM-34548 (R.R.B.) and EY-11256 (B.E.K.) and the W. M. Keck Center for Molecular Electronics at Syracuse University.

* To whom correspondence should be addressed. R.R.B.: telephone, (860) 486-6720; fax, (860) 486-2981; e-mail, rbirge@uconn.edu. B.E.K.: telephone, (315) 464-8719; fax, (315) 464-8750; e-mail, knoxb@mail.upstate.edu.

‡ University of Connecticut.

§ Syracuse University.

|| Present address: Jules Stein Eye Institute, 100 Stein Plaza, University of California, Box 957000, Los Angeles, CA 90095-7000.

⊥ State University of New York Upstate Medical University.

@ Present address: Department of Biological Chemistry and Molecular Pharmacology, Harvard Medical School, 240 Longwood Ave., Boston, MA 02115.

[1] Abbreviations: VCOP, *Xenopus laevis* violet cone opsin; ROS, rod outer segments; rho or s. rho, solubilized rhodopsin; LM, *N*-dodecyl *β*-D-maltoside; HEPES, *N*-(2-hydroxyethyl)piperazine-*N*′-2-ethanesulfonic acid; SB, Schiff base; PSB, protonated Schiff base; PSS, photostationary state; PSS$\lambda\lambda\lambda$, photostationary state generated with illumination at wavelength $\lambda\lambda\lambda$ in nanometers; $\mathbf{B_1}$, primary photostationary state of VCOP at cryogenic temperatures; $\mathbf{B_2}$, red-shifted photostationary state generated upon extended photochemical excitation of the $\mathbf{B_1}$ state at certain temperatures; *batho*, *lumi*, *meta I*, and *meta II*, discrete thermal intermediates of the visual opsin bleaching pathway.

10.1021/bi010387y CCC: $20.00
Published on Web 06/07/2001

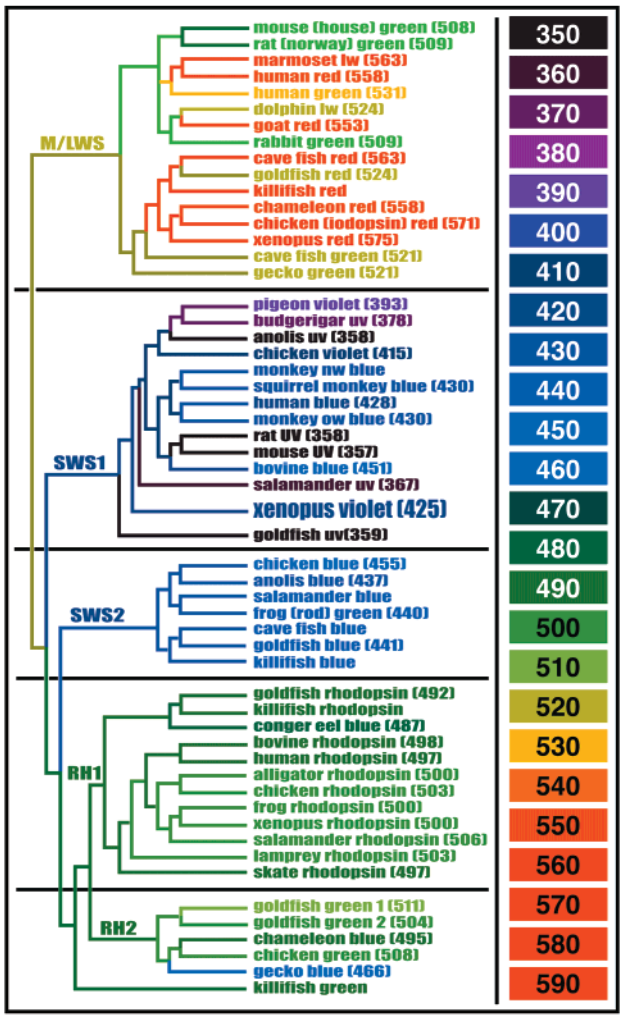

FIGURE 1: Dendogram of selected vertebrate visual opsins. Absorption maxima when known are shown within parentheses in nanometers, and the text is displayed in color based on the wavelength (nanometers) template shown in the column at right. The *X. laevis* violet cone opsin (VCOP) is labeled "xenopus violet" and is shown in enhanced type in the SWS1 group. The VCOP pigment absorbs maximally at 425 nm when regenerated with 11-*cis*-A_1-retinal, an absorption maximum nearly identical to that of the human blue cone. This figure was adapted from Figure 3 of the review by Ebrey and Koutalos (*13*), with additional or updated SWS1 pigment data from refs *14*−*20*.

important role in determining the signal amplification, recovery, and response kinetics of the rod and cone photoreceptor cells. The intermediates in the photobleaching pathway of rod and cone opsins can be thermally trapped and detected by observing changes in the UV−vis spectrum. This approach has been used extensively to study the pathways of several pigments and to understand the molecular basis of rod and cone opsin function (*21*−*27*). The relatively small number of studies on group SWS1 pigments is due in part to the difficulty of obtaining sufficient quantities of stable pigments (*12*, *14*, *28*−*35*). Our expression and isolation protocol yields sufficient quantities of the *Xenopus* violet cone opsin (VCOP) (*14*, *36*) to permit detailed biochemical and spectroscopic study.

All of the pigments in the M/LWS, RH1, RH2, and SWS2 groups are red-shifted relative to a protonated Schiff base in solution (λ_{max} = 400−440 nm) and presumably have a protonated Schiff base linkage in the dark state. In contrast, some of the SWS1 group pigments exhibit absorption maxima blue-shifted relative to that of a protonated Schiff base in solution. Some pigments have absorption maxima in the UV (~370 nm), while others absorb in the violet (410−450 nm). The separation of the pigments into two wavelength distributions suggests that the UV pigments have a deprotonated Schiff base whereas the violet cones have a protonated Schiff base in the dark (*14*).

In the study presented here, we use the low-temperature trapping method to investigate the photobleaching pathway of the violet cone opsin. We supplement these results with the use of FTIR spectroscopy to determine the protonation state of the chromophore, and semiempirical (MNDO-PSDCI) and ab initio (B3LYP/6-31G) molecular orbital theory to analyze the protein binding site and the mechanism of wavelength regulation.

MATERIALS AND METHODS

Expression, Isolation, and Purification of the Visual Pigments. An expression construct, pMT-VCOP, containing the first 328 codons of the *Xenopus* violet cone opsin coding region and the last 14 codons of bovine rod opsin was expressed in mammalian COS1 cells by transient transfection (*14*, *35*, *36*). The violet cone opsin was regenerated with 11-*cis*-A_1-retinal and purified by column immunoaffinity chromatography on 1D4-Sepahrose. Fractions that contained the visual pigment were collected from the column and concentrated to a final A_{425} of ~0.3 using a Centricon C-30 filter (Millipore, Bedford, MA). The rhodopsin E113Q mutant was expressed in mammalian COS1 cells, isolated, and purified in the same manner (*37*). Rhodopsin was solubilized (s. rho) and purified from rod outer segments (ROS) by using immunoaffinity chromatography on concanavalin A−Sepharose (*38*). All pigments were stored at −80 °C until they were used.

Violet Cone Opsin Studied by Cryogenic Electron Spectroscopy. Visual pigment samples were mixed with glycerol to produce a 67% glycerol and 0.05% *N*-dodecyl *β*-D-maltoside (LM, Anatrace, Maumee, OH) solution in buffer A [50 mM HEPES, 140 mM NaCl, and 3 mM $MgCl_2$ (pH 6.8)]. Samples for cryogenic studies at 45−200 K were placed in an Air Products Displex helium-refrigerated cryostat coupled to a Shimadzu 3101 UV−vis−NIR spectrophotometer as previously described (*14*). Samples for the studies at 230−273 K were placed in a Varian Cary 3E UV−vis spectrophotometer modified to allow accurate temperature control from 228 to 280 K, thus enabling the stabilization of the later intermediates via temperature trapping.

The sample was illuminated with a Photomax system equipped with a 200 W arc lamp coupled to a monochromator (Oriel, Stratford, CT). A photostationary state (PSS) was generated by successive illuminations until no further spectral changes could be detected (~1 h, unless specified otherwise). In the subsequent discussion, the wavelength of illumination in nanometers used to generate the photostationary state is indicated following the PSS abbreviation.

All the electronic spectra are the average of four spectra at each temperature normalized with respect to the protein aromatic residue band at 280 nm (A_{280}). Each photostationary state described in this paper was reproduced two to four times from independent transfections. Each of the difference spectra

was calculated by subtracting the appropriate photostationary state from the corresponding dark or previous photostationary state.

FTIR Difference Spectroscopy of the Visual Pigments. FTIR samples had the glycerol and HEPES removed and the concentration of LM decreased by exchanging buffer A with buffer B [10 mM potassium phosphate buffer (pH 6.8) and 0.02% LM] using Centricon C-30 filters. The buffer A in which E113Q was purified was exchanged for buffer C [10 mM potassium phosphate buffer (pH 8.2) and 0.02% LM]. Excess 1D4 peptide was removed from the samples by passing the pigments over prepacked Sephadex G-50 columns (Pharmacia, Peapack, NJ). The final concentration of the samples was adjusted to 1 μg/μL. Deuterated samples were prepared by following the above procedure using buffer B or C prepared with D_2O.

The pigment (~100 μg) was dried on an infrared quality CaF_2 window under a continuous stream of nitrogen. The film was sealed with another CaF_2 window and mounted on a Nicolet Magna IR 750, series II instrument (Nicolet Instrument Corp., Madison, WI). The protein samples were equilibrated at 263 K for approximately 1 h. The dark state spectra of the pigments were obtained by collecting and averaging 512 scans. Illuminating the sample from an appropriately filtered 250 W quartz halogen lamp (3−5 min) at 263 K generated the active state of the proteins. The rhodopsin *meta II* intermediate was generated using a 495 nm cutoff filter (Melles Griot 03FCG067). The violet cone opsin *meta II* intermediate was generated using a 395 nm cutoff filter (Melles Griot 03FCG055), and the E113Q *meta II* intermediate was generated using a 305 nm cutoff filter (Melles Griot 03FCG121). The *meta II* spectra of the pigments were obtained by collecting and averaging 512 scans (~8 min). The samples were illuminated for an additional 2−3 min, and the spectra were collected. Data collection and analysis were performed using OMNIC 3.1 (Nicolet Instrument Corp.). Each difference spectrum was calculated by subtracting the spectrum for the *meta II* intermediate from the spectrum from the appropriate dark state. The resulting difference spectra from the second illumination were identical to that of the first illumination, indicating the complete formation of the photoproduct at 263 K. The raw spectra have not been corrected for baseline deviations, but have been smoothed using a three-point triangular slit function.

Theoretical. The ground state vibrational properties of model chromophores were calculated using both Hartree−Fock and density functional (B3LYP) ab initio molecular orbital theory and basis sets up to 6-31G(d) via Gaussian 98 (*39*). The relevant details will be reported below. The spectroscopic properties of the protein-bound chromophore were calculated using MNDO-PSDCI molecular orbital theory, including full single and double configuration interaction within the chromophore π-electron manifold (*40*). This method allows the entire protein binding site to be included in the SCF calculation while constraining the configuration interaction to the chromophore. However, when dispersive interactions between the chromophore and nearby aromatic residues are of interest, single and double CI is extended to include the aromatic residues. (Dispersive interactions can be simulated theoretically by using double CI where the coupled excitations on both the chromophore and residue are included.) Although we have developed spectroscopic parametrizations that work with the MNDO, AM1, or PM3 Hamiltonians, we have found that the PM3 Hamiltonian, which will be adopted in this study, provides the best agreement with experiment when simulating the protein binding sites of both bacteriorhodopsin and rhodopsin (*14*, *40*−*47*).

Spectrum #	Illumination			$T_{spectrum}$ (K)
	λ_{ill} (nm)	T_{ill} (K)	t_{ill} (hr)	
1	-	-	0	45
2	395	45	1	45
3	-	-	0	200

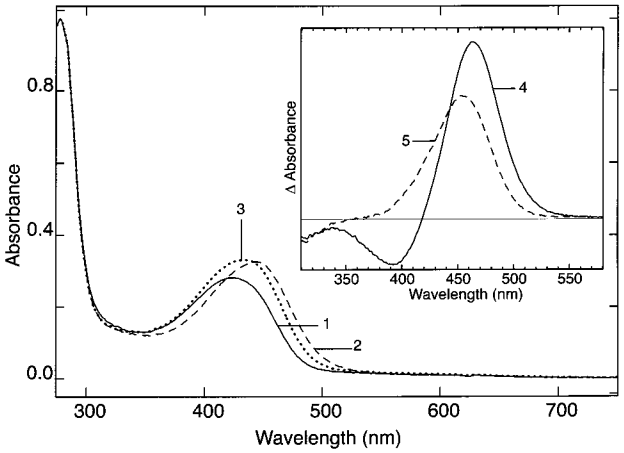

FIGURE 2: Photochemistry of the violet cone opsin at 45 K. The **B_1** state generated at 45 K (spectrum 2) is stable to 198 K, but decayed to the *lumi* intermediate at 200 K (spectrum 3). The table lists the conditions under which the spectra were collected, where λ_{ill} is the wavelength of light (in nanometers) used to generate the photoproduct, T_{ill} is the temperature at which the illumination was performed (in kelvin), t_{ill} is the length of illumination (in hours), and $T_{spectrum}$ is the temperature at which each spectrum was collected. Dashes indicate no change from the previous conditions (i.e., no further illumination, or no change in temperature). The difference spectra are shown in the inset. Curves 4 and 5 correspond to spectrum 2 and spectrum 3 minus spectrum 1, respectively.

RESULTS

Batho Intermediate of the Violet Cone Opsin. Previously, we observed two *batho*-shifted photostationary intermediates for VCOP at very low temperatures (*14*). In the study presented here, we investigated the behavior of the two states upon warming. We initially formed the photostationary state (**PSS395**) at 45 K (Figure 2, spectrum 2) which was identical to the one previously observed (called XB_{30K} in ref *14*). Henceforth, we will call this photostationary state **B_1**. When **B_1** is warmed to 75 K and thermally equilibrated for 12 h, no spectral change is observed (data not shown). Therefore, **B_1** cannot be converted thermally to the second *batho*-like intermediate previously observed (called XB_{70K} in ref *14*), and henceforth called **B_2**. Furthermore, no change in the **B_1** spectrum is detected until the next thermal intermediate is formed at 200 K (Figure 2, spectrum 3). The 395 nm photostationary state (**PSS395**) is usually reached within 20−30 min at 45 K. However, because of the high concentrations of protein used in this study, illumination was carried out for longer times (1 h) to make sure that the maximum amount of *batho* product was formed. At 45 K, continued illumina-

Spectrum #	Illumination			$T_{spectrum}$ (K)
		T_{ill} (K)	t_{ill} (hr)	
1	-	-	0	75
2	395	75	1	75
3	395	75	12	75
4	-	-	0	45

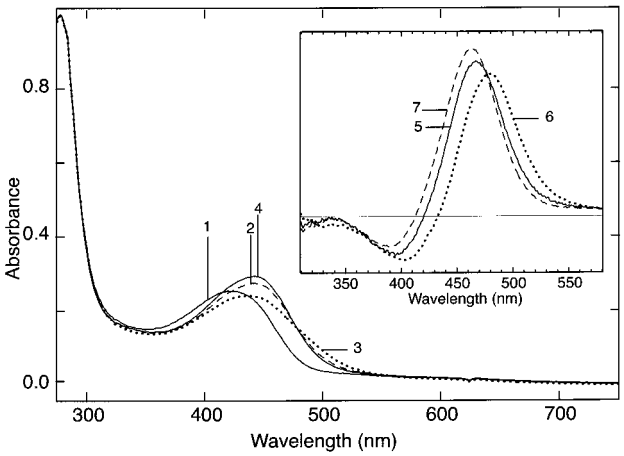

FIGURE 3: Photochemistry of the violet cone opsin at 75 K. The formation of the $\mathbf{B_1}$ state at 75 K was observed at early illumination times (spectrum 2), provided that the protein was in the dark form. Extended illumination at 75 K generated the $\mathbf{B_2}$ state (spectrum 3). $\mathbf{B_2}$ was not stable at low temperatures, and blue-shifted at 45 K (spectrum 4). The table lists the conditions under which the spectra were collected using the same scheme outlined in the legend of Figure 2. The difference spectra are shown in the inset. Curves 5−7 correspond to spectra 2−4 minus spectrum 1, respectively.

tion (2−12 h) of $\mathbf{B_1}$ does not result in any further spectral shift, thus ruling out the formation of a low-quantum efficiency product at this temperature. However at 75 K, depending on the chromophore composition of the initial dark state, $\mathbf{B_2}$ is formed within 1 h of illumination or after 12 h of illumination. If formation of $\mathbf{B_2}$ is a low-quantum efficiency event, then we would expect that the time required to form $\mathbf{B_2}$ at 75 K would be independent of the chromophore composition of the dark state at 75 K, which is not the case.

We carried out a series of experiments to probe the nature of $\mathbf{B_1}$ and $\mathbf{B_2}$ in more detail, and the spectroscopic results are shown in Figures 3 and 4. Because $\mathbf{B_2}$ was originally observed following irradiation at 75 K, we investigated whether $\mathbf{B_1}$ could also be formed at 75 K. A careful set of experiments as a function of irradiation time at 75 K indicates that $\mathbf{B_1}$ not only forms at this temperature but also is the initial product observed at short irradiation times. Illumination of a dark sample at 75 K with 395 nm light for ~1 h results in the formation of $\mathbf{B_1}$ (Figure 3, spectrum 2). However, prolonged illumination (~12 h) results in the formation of $\mathbf{B_2}$ (Figure 3, spectrum 3). Interestingly, when $\mathbf{B_2}$ is cooled to 45 K, the spectrum blue shifts to a spectrum very similar to that of $\mathbf{B_1}$ (Figure 3, spectrum 4). This behavior is reminiscent of the *batho* intermediate formed at low temperatures from iodopsin (chicken red), which displays a *batho* intermediate that blue shifts back to the original dark spectrum upon warming (*48*). In other experiments, we found that warming $\mathbf{B_2}$ to 140 K results in a blue-shifted spectrum identical to that of $\mathbf{B_1}$ (data not shown). To investigate this phenomenon further, the following experiments were carried out. A dark sample (Figure 4, spectrum 1) was illuminated at 45 K to generate $\mathbf{B_1}$ (Figure 4, spectrum 2). The photostationary state mixture was then gradually warmed to 140 K, and illuminated with 500 nm light to generate **PSS500**. The resulting spectrum (Figure 4, spectrum 3) was nearly identical to the original dark spectrum (Figure 3, spectrum 1). Illumination of **PSS500** with 395 nm light at 140 K results in the formation of a red-shifted species (Figure 4, spectrum 4) that is virtually identical to $\mathbf{B_1}$ (Figure 4, spectrum 2). This red-shifted species was illuminated with 500 nm light to generate **PSS500** at 140 K. The **PSS500** mixture was then cooled to 75 K (Figure 4, spectrum 5) and illuminated with 395 nm light to generate a red-shifted **PSS395** species very similar to $\mathbf{B_2}$ (Figure 4, spectrum 6). Warming this **PSS395** species (Figure 4, spectrum 6) gradually to 140 K results in a blue-shifted species (Figure 4, spectrum 7) that is similar to $\mathbf{B_1}$. Further warming the mixture subsequently forms the next thermally stable intermediate (*lumi*) at 200 K (data not shown).

Studies on the chicken red pigment indicate that increasing the temperature of the *batho* photostationary state regenerates the original dark spectrum (*49*, *50*). Extraction studies confirm that increasing the temperature induces a thermal isomerization of the chromophore from all-*trans* to 11-*cis* (*49*, *50*). In contrast, the *batho* PSS of VCOP displays no spectral shifts upon warming from 45 to 198 K, and we conclude that the amount of the all-*trans* chromophore remains constant during this temperature increase. Also in chicken red, it has been shown that the 9-*cis* isomer formed at 77 K is stable and does not undergo any significant isomerization upon warming (*49*, *50*). Previously, Vought et al. (*14*) have shown that when dark VCOP is cooled to 77 K, rewarming and extracting the chromophore results in predominantly the 11-*cis* isomer, ruling out any significant isomerization of the 11-*cis* form during the temperature ramping. Thus, all these observations justify our assumption that the chromophore isomer composition remains constant during the temperature ramping experiments.

It is clear from our experiments that $\mathbf{B_2}$ is formed via a side reaction that is not part of the main pathway. Therefore, we identify the $\mathbf{B_1}$ photostationary state as one containing the primary photochemical intermediate and conclude that $\mathbf{B_2}$ is generated via a process that involves a change in protein conformation not relevant to the thermal pathway observed during the photobleaching sequence. The nature of the reversal from $\mathbf{B_2}$ back to $\mathbf{B_1}$ upon cooling is discussed in greater detail in the Discussion.

Later Intermediates of the Violet Cone Opsin. The $\mathbf{B_1}$ spectrum (λ_{max} = 450 nm) is slightly blue-shifted at 200 K, but remains red-shifted relative to that of the dark state (λ_{max} = 425 nm). This spectral behavior is characteristic of the *lumi* intermediate (λ_{max} = 435 nm) (Figure 2, spectrum 3, and Figure 5, spectrum 2). Once formed, the *lumi* intermediate is stable up to 228 K.

The *meta I* and *meta II* intermediates of the sequence were trapped at various temperatures after formation of the *lumi* intermediate at 228 K (Figure 5, spectrum 2). Increasing the temperature to 253 K broadened and blue-shifted the spectrum (Figure 5, spectrum 3), indicating the presence of the *lumi* and *meta I* intermediates. Increasing the temperature to 258 K initiates the slow decay of the mixture (Figure 5C). The difference spectra were calculated by subtracting individual, successive spectra at 258 K from the dark state

Spectrum #	Illumination			$T_{spectrum}$ (K)
		T_{ill} (K)	t_{ill} (min)	
1	-	-	0	45
2	395	45	1	45
3	500	45	1	140
4	395	140	1	140
5	500	140	1	75
6	395	75	1	75
7	-	-	0	140

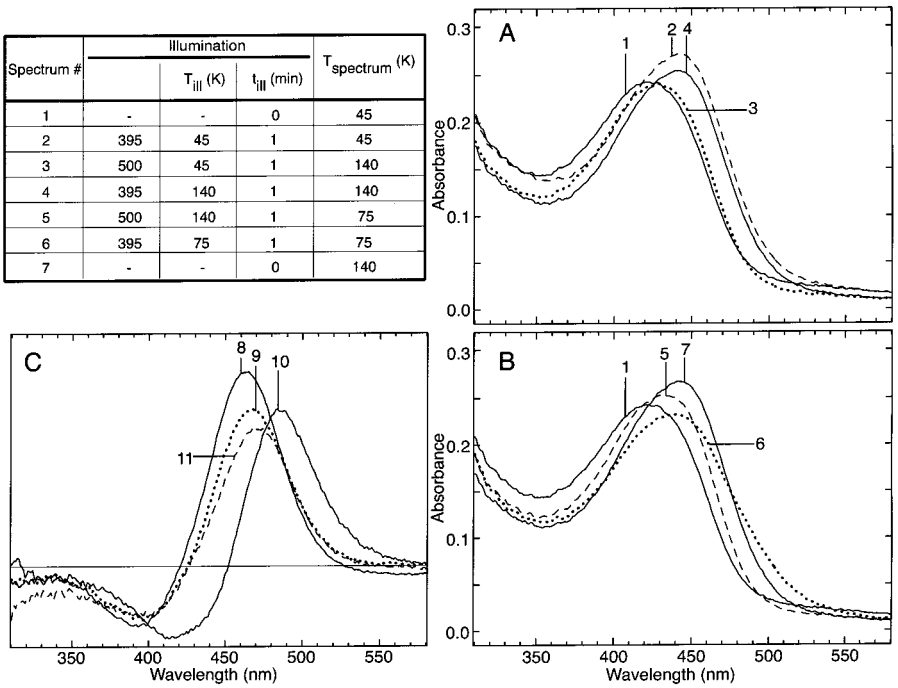

FIGURE 4: Photochemistry of the violet cone opsin at 45, 75, and 140 K. The $\mathbf{B_1}$ state was generated at 45 (spectrum 2) and 140 K (spectrum 4) by illuminating at 395 nm for ~1 h. $\mathbf{B_1}$ was driven back with 500 nm light at 45 (spectrum 3) and 140 K (spectrum 5). The $\mathbf{B_1}$ PSS at 75 K cannot be detected after formation of **PSS500** at 140 K. Instead, a red-shifted state (relative to $\mathbf{B_1}$), $\mathbf{B_2}$, was generated (spectrum 6). The $\mathbf{B_2}$ PSS was not stable at higher temperatures, and decayed back to the $\mathbf{B_1}$ PSS (spectrum 7). The table lists the conditions under which the spectra were collected using the same scheme outlined in the legend of Figure 2. The difference spectra are shown in panel C. Curve 8 corresponds to spectrum 2 minus spectrum 1. Curve 9 corresponds to spectrum 4 minus spectrum 3. Curve 10 corresponds to spectrum 6 minus spectrum 5. Curve 11 corresponds to spectrum 7 minus spectrum 5.

Spectrum #	Illumination			$T_{spectrum}$ (K)
	λ_{ill} (nm)	T_{ill} (K)	t_{ill} (hr)	
1	-	-	0	228
2	395	228	1	228
3	-	-	0	253
4	-	-	0	263

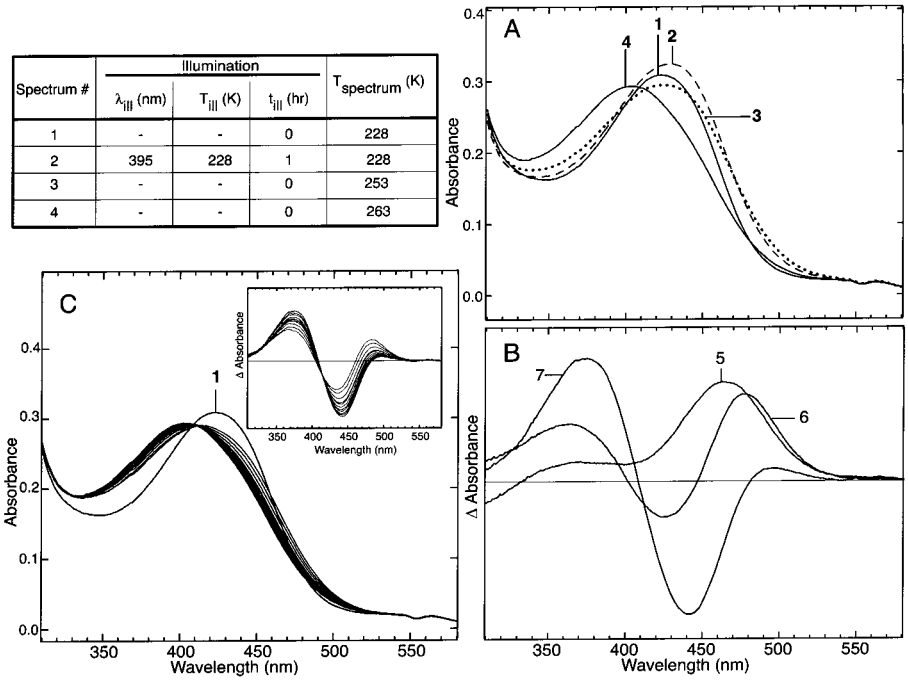

FIGURE 5: Formation of the latter intermediates of the violet cone opsin. The *lumi* intermediate formed at 228 K (spectrum 2) and decayed without further illumination to a mixture of *lumi* and *meta I* at 253 K (spectrum 3). The mixture started to decay to the *meta II* intermediate at 258 K. The transition took ~4 h for completion. The spectra in panel C were collected in 20 min intervals at 258 K. The inset in panel C shows the spectra at 258 K minus the spectra of the dark state (spectrum 1). The table lists the conditions under which the spectra were collected using the same scheme outlined in the legend of Figure 2. The difference spectra are shown in panel B. Curves 5−7 correspond to spectra 2−4 minus spectrum 1, respectively.

spectrum at 228 K (Figure 5C, inset). Increasing the temperature to 263 K did not affect the spectrum in any appreciable way (Figure 5, spectrum 4). The difference spectra of the *lumi* intermediate, the *lumi*/*meta I* mixture, and the *meta II* intermediate minus the dark state spectrum are shown in Figure 5B.

Spectra of the pure intermediates were calculated by using the HPLC data to assign the isomer composition of the $\mathbf{B_1}$

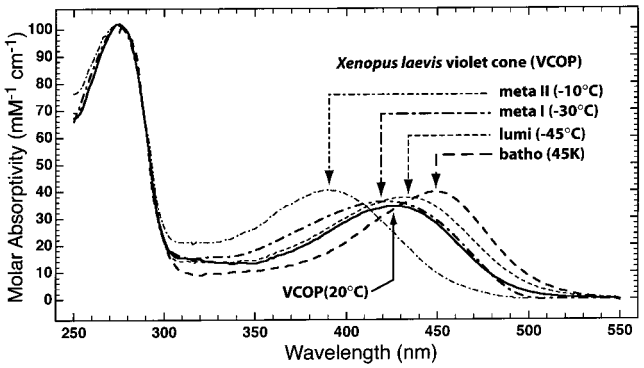

FIGURE 6: Electronic absorption spectra of the violet cone opsin and its key photobleaching intermediates. The spectra are generated via decomposition of the temperature-trapped photostationary state spectra, and each is measured at the temperature indicated in the legend. The arrowheads point to the absorption maxima.

state, and assuming that the amount of the dark (11-*cis* and 9-*cis*) states remained constant during the temperature ramping experiments described above. Decomposition into pure components was straightforward for all species except *meta I*, which had an uncertainty of ±5% with respect to *lumi* contamination. The spectra of the VCOP intermediates and a comparison of the photobleaching sequence of VCOP and rhodopsin are presented in Figures 6 and 7. We will return to a more detailed discussion of the data presented in these figures in the Discussion.

FTIR Difference Spectroscopy of the Visual Pigments. FTIR difference spectroscopy monitors the molecular vibrations of specific groups between a photoproduct and the dark state of a protein. The FTIR difference spectra of the *meta II* minus the spectra of the dark states of rhodopsin (s. rho and ROS), the rhodopsin counterion mutant (E113Q at pH 8.2), and the violet cone opsin at 263 K are shown in Figure 8. The rhodopsin FTIR difference spectrum was used because rhodopsin has been shown to contain a protonated Schiff base linkage in the dark state, while at pH 8.2, E113Q is unprotonated. The rhodopsin difference spectra in H_2O and D_2O are in agreement with the previously published spectra, and the E113Q difference spectra are very similar to those of the previously studied E113A mutant (*51*−*54*).

The difference spectra of the violet cone opsin in H_2O and D_2O represent the first FTIR study of a vertebrate short-wavelength cone pigment. The amide I (C═O peptide stretch) and amide II (N−H peptide bend coupled to the C−N peptide stretch) bands absorb between 1690 and 1620 cm^{-1} and between 1570 and 1500 cm^{-1}, respectively. Large changes observed in the difference spectrum in these regions reflect the rearrangement of the protein backbone during the formation of the active state. The bands at 1652 and 1640 cm^{-1} in the rhodopsin difference spectrum are due to amide I vibrations. Previous reports and our observations have shown that the bands in this region are highly dependent on the sample preparation (data not shown) (*54*). The Schiff base stretching frequency in proteins is located at ∼1650 cm^{-1} (*54*, *55*). However, due to the high band variability in this region, a conclusive assignment of the prominent VCOP band at ∼1660 cm^{-1} is difficult.

The intense bands between 1570 and 1500 cm^{-1} in the rhodopsin spectrum are due to the C═C stretching vibrations of the chromophore (*56*). The polyene bands in the rhodopsin

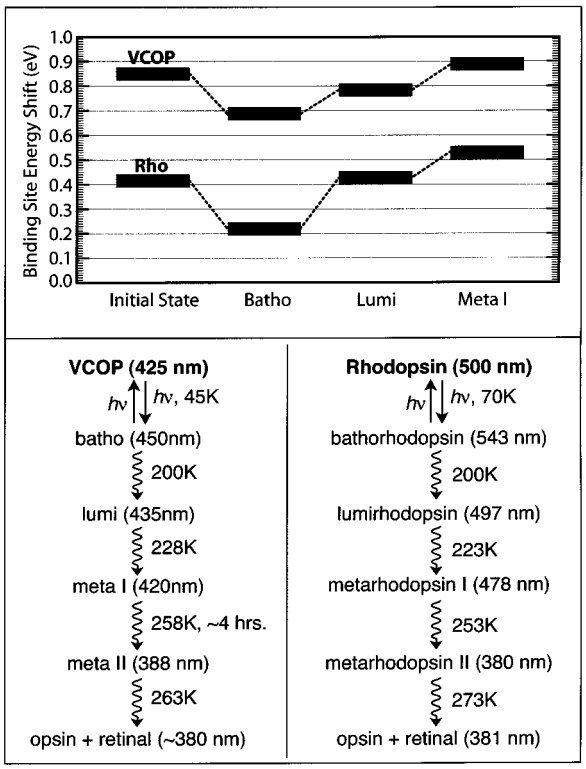

FIGURE 7: Comparison of the photobleaching sequences of the *Xenopus* violet cone opsin and rhodopsin. The plot at the top shows the blue shift associated with incorporation of a hypothetical all-*trans* protonated Schiff base chromophore ($\lambda_{max} \approx 600$ nm) into the protein binding site for the protonated intermediates. The lower left column shows the photobleaching sequence of VCOP. Illumination of the dark state generates the *batho* intermediate ($\lambda_{max} = 450$ nm). The *batho* intermediate decays thermally to the *lumi* intermediate ($\lambda_{max} = 435$ nm) at 200 K. At 258 K, the *meta I* intermediate ($\lambda_{max} = 420$ nm) is formed. The transition to the *meta II* intermediate ($\lambda_{max} = 388$ nm) begins to occur at 258 K and is complete after 4 h at 258 K. Finally, the *meta II* state decays to free retinal and opsin. The photobleaching sequence of bovine rhodopsin is shown in the lower right column. Straight arrows designate light-activated transitions, whereas wavy arrows designate thermally driven transitions.

difference spectrum are at 1530 (+) and 1557 (−) cm^{-1} [henceforth, we refer to the negative bands with (−) and the positive bands with (+)]. The polyene chromophore bands in the E113Q mutant spectrum are located at 1550 (+) and 1560 (−) cm^{-1}. The VCOP spectrum only has two bands at 1538 (−) and 1550 (+) cm^{-1}. These two bands can be tentatively assigned to the chromophore C═C stretches on the basis of the position of the chromophore C═C stretches in rhodopsin and the E113Q mutant, the intensity of the bands, and the lack of other bands in this region. Note that these bands in the VCOP spectrum are inverted when compared to the bands in the rhodopsin and E113Q spectra. Despite the large difference in the absorption maxima of rhodopsin ($\lambda_{max} = 500$ nm) and E113Q ($\lambda_{max} = 380$ nm) and the *meta II* state ($\lambda_{max} = 381$ nm), the ordering of the C═C bands in rhodopsin and E113Q is the same. The inversion of the VCOP bands assigned to the C═C chromophore stretches suggests that the binding site in the violet cone opsin is significantly altered when compared to the rhodopsin and E113Q binding sites. The bands arising from the chromophore in the fingerprint region and the C═O stretching modes of carboxylic acids are examined below.

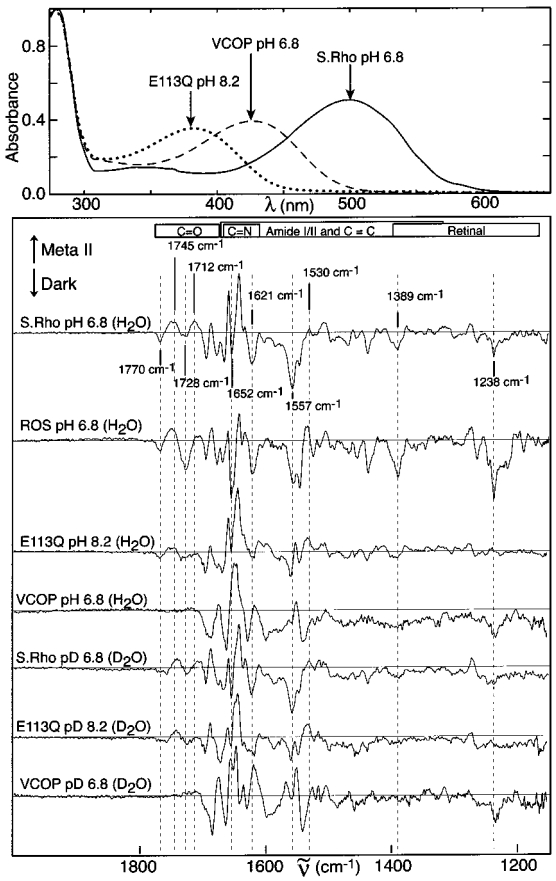

FIGURE 8: FTIR difference spectra of the *meta II* intermediate spectrum minus the rhodopsin (s. rho and ROS), E113Q, and VCOP dark state spectra in H_2O and D_2O. The graph at the top shows the room-temperature absorption spectra of the three pigments that were examined. E113Q at pH 8.2 was selected because it contains an unprotonated Schiff base chromophore. All the FTIR spectra were collected at 263 K, and the pH of each sample is indicated in the label. The dotted lines and frequencies noted represent the position of bands in the solubilized rhodopsin spectrum in H_2O at pH 6.8. Literature assignments of the rhodopsin bands are as follows: 1238 cm^{-1} ($C_{12}-C_{13}$, $C_{10}-C_{11}$, $C_{14}-C_{15}$, and $C_{15}-H$ coupled mode, and N−H bending modes) (*62*−*64*), 1530 and 1557 cm^{-1} (C═C chromophore stretches) (*56*), 1655 cm^{-1} (amide I, C═N−H stretches) (*62*), 1712 cm^{-1} (E113 carbonyl stretch) (*71*), 1728 cm^{-1} (E122 carbonyl stretch and the ester C═O stretch of phospholipids) (*56*, *70*), 1745 and 1770 cm^{-1} (D83 carbonyl stretch) (*52*, *69*).

DISCUSSION

We studied the formation and decay of all the intermediates of VCOP that were trapped from 45 to 280 K. Thus, while we were able to characterize the *batho*, *lumi*, *meta I*, and *meta II* intermediates, the possible existence of a blue-shifted intermediate (*57*) was not studied. At 45 K, the primary photochemical intermediate, *batho*, is formed. The *batho* intermediate (all-*trans*-retinal bound to opsin) is red-shifted with respect to the dark state (11-*cis*-retinal bound to opsin) and is the principal component of the primary photostationary state, $\mathbf{B_1}$. The $\mathbf{B_1}$ PSS generated at 45 K is stable from 45 to 198 K (Figures 2 and 3). Light activation at 140 K also generates the *batho* intermediate, which is stable to 198 K (data not shown). At 200 K, the *batho* intermediate decays to the *lumi* intermediate (see below) as expected.

The violet cone opsin exhibits unique photochemistry at 75 K. Illuminating the (dark) violet cone opsin at 75 K generates the $\mathbf{B_1}$ PSS within 1 h (Figure 4, spectrum 2), but extended illumination (~12 h) at 75 K accesses a state even further red-shifted, the $\mathbf{B_2}$ state (Figure 4, spectrum 3). The $\mathbf{B_2}$ PSS is also accessible when the violet cone opsin **PSS500** (50% 11-*cis*-, 11% all-*trans*-, and 39% 9-*cis*-retinal) is illuminated with 395 nm light for approximately 1 h at 75 K. Despite the identical, or nearly identical, chromophore compositions of the two photostationary states, the $\mathbf{B_2}$ state (whose λ_{max} can vary between 460 and 480 nm depending upon how it is generated) is significantly red-shifted from the $\mathbf{B_1}$ PSS ($\lambda_{max} \approx 460$ nm). $\mathbf{B_2}$ generated from **PSS500** reverts to the $\mathbf{B_1}$ PSS upon increasing the temperature to 140 K (Figure 4) or decreasing the temperature to 45 K (Figure 3). Scheme 1 depicts the formation of the photoproduct at 75 K using short-term illumination ($\mathbf{B_1}$), followed by extended illumination ($\mathbf{B_2}$), and finally the change in temperature to 140 and 45 K.

We have indicated the absorption maxima (λ_{max}), or in the case of photostationary states, the difference maxima (λ_{diff}), in parentheses. The absorption spectra of the *batho* (pure all-*trans* species) photoproducts were generated via deconvolution based on the HPLC data. A key point of Scheme 1 is that the isomer compositions of the $\mathbf{B_1}$ and $\mathbf{B_2}$ photostationary states are identical within experimental error. (Measurements of the isomer composition differed by ±5%, and the values shown in Scheme 1 are rounded to ±10%.) This observation places important constraints on the nature of these photostationary states and the origin of the spectral differences.

One possible explanation for $\mathbf{B_2}$ worth considering is that at 75 K, the residues in the binding site are able to move to a higher-energy conformation, allowing the all-*trans* chromophore to relax into a more planar conformation. The more planar chromophore has less single-bond torsional distortion which lowers the energy of the excited state more than that of the ground state, and therefore leads to a longer-wavelength absorption maximum. However, the observation that $\mathbf{B_2}$ reverts to $\mathbf{B_1}$ when the temperature is both increased to 140 K or decreased to 45 K indicates that the system is not in equilibrium. We hypothesize that the total free energy of the $\mathbf{B_2}$ PSS is higher than that of the $\mathbf{B_1}$ PSS, because of the distortion of the binding site rather than distortion of the long, and relatively flexible, retinyl chromophore. The metastable $\mathbf{B_2}$ PSS should be quite sensitive to conditions that alter the strain energy of the system, which would include cooling. This explanation suggests that site-directed mutations of the binding site would influence the properties of both $\mathbf{B_1}$ and $\mathbf{B_2}$. Indeed, we have found one mutant, S85D, which displays only a single bathochromically shifted photostationary state with a wavelength maximum roughly intermediate between those of $\mathbf{B_1}$ and $\mathbf{B_2}$ (manuscript in preparation).

The *lumi* intermediate ($\lambda_{max} = 435$ nm) is formed at 200 K via the thermal decay of the *batho* intermediate and is stable up to 228 K (Figures 2 and 5). The transition to the *meta I* intermediate starts occurring at 253 K (Figure 5, spectrum 3). The *meta I* spectrum is very broad and may be contaminated with the *lumi* intermediate that has not decayed completely at 253 K. Increasing the temperature to 258 K destabilizes the *meta I* intermediate, and it decays to the *meta II* intermediate in approximately 4 h (Figure 5C). The formation of the *meta II* intermediate is complete after 4 h

Scheme 1

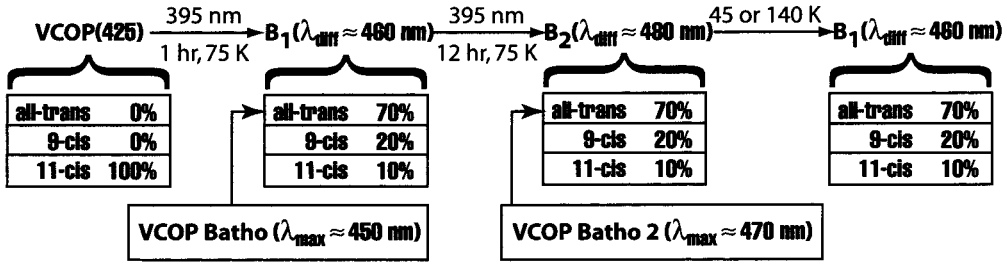

at 258 K, and increasing the temperature to 263 K does not produce any further changes in the spectrum (Figure 5).

It has been difficult to determine when the retinal is released from the photolyzed VCOP. Although acid denaturation has become a standard method for denaturing the *meta II* state of bovine rhodopsin to form a product that contains a stable protonated retinylidene Schiff base linkage to opsin (*58*), many attempts to obtain a similar species with light-exposed VCOP have failed (data not shown). This failure is somewhat surprising because VCOP can be acid denatured in the dark, producing a species very similar to the one formed by bovine rhodopsin (*35*). Thus, it appears that the unprotonated Schiff base in VCOP is quite unstable and undergoes rapid hydrolysis during protein denaturation. Biochemical assays employing light-dependent transducin activation, which are used to evaluate the light-activated form R* and presumably *meta II*, indicate that the VCOP *meta II* lifetime is approximately 2 min at ~300 K (*35*). At lower temperatures, *meta II* is likely to be more stable. The FTIR spectra at 263 K are also consistent with a stable *meta II* state at this temperature (see below). Therefore, we conclude that the VCOP *meta II* is stable at <273 K.

The photobleaching pathway of the violet cone opsin is remarkably similar to that of rhodopsin (Figure 7). The similarity is best illustrated by the wavelength regulation associated with each of the photobleaching intermediates when plotted in terms of the blue shift associated with protein−chromophore stabilization (Figure 7, top). We arbitrarily set the transition energy of the vacuum state of the PSB at 600 nm, but note that this value is not relevant to the relative shifts, which are the meaningful data. What is clear from examination of Figure 7 is that while the photobleaching sequence is blue-shifted in VCOP relative to that in rhodopsin, the protein−chromophore interactions that are responsible for the photobleaching pathway are remarkably similar with respect to the chromophore−protein interactions, the conformational changes of the chromophore, or both.

Protonation State of the Chromophore

To characterize the protonation state of the chromophore in VCOP, we have compared the VCOP difference spectrum to two the spectra of previously well characterized proteins, rhodopsin and its counterion mutant, E113Q. We have determined the difference spectrum between dark and *meta II*, the deprotonated intermediate (*59*). We examine three regions of the spectrum that are characteristic of a deprotonation event between these two states: the chromophore bands in the fingerprint region, the C═N stretching region, and the carboxylic acid stretching region.

The fingerprint region (1400−1100 cm^{-1}) of VCOP shows a prominent 11-*cis* chromophore band in the dark state at 1232 cm^{-1}, as found in rhodopsin at 1238 cm^{-1} (*55*, *60*−*64*). The negative band at 1238 cm^{-1} represents a complex, delocalized mode of the chromophore involving the C−C stretching, C−H bending, and N−H bending of the Schiff base region (despite the contribution of other modes, we will refer to this band as the chromophore C−C stretches; see below) (*62*, *64*). Previous studies with rhodopsin and model compounds have shown that protonated Schiff bases have increased band intensities in this region when compared to that of the unprotonated Schiff base (*65*). The increase in band intensity has been attributed to the reduced number of bond alterations but increased number of charge alterations on the carbon atoms of the chromophore due to π-electron delocalization (*65*). E113Q at pH 8.2 does not exhibit a band at ~1238 cm^{-1}, consistent with the absence of a protonated SB linkage in this form of the counterion mutant (Figure 8). The downshift to 1232 cm^{-1} in the VCOP difference spectrum suggests that the Schiff base environment in the VCOP is different from the environment of the rhodopsin chromophore. A similar downshift is seen in the protonated rhodopsin E113A mutant (*54*, *66*, *67*).

The protonation state of the chromophore in rhodopsin has been characterized by the C═N stretching frequency (*51*, *54*). However, the C═N region in the VCOP spectra also contains vibrations due to the amide I band, which makes assigning the C═N stretching frequency with certainty very difficult. Further characterization of this region in VCOP would require the use of labeled chromophores (*68*).

The C═O stretching modes of carboxylic acids in the protein are located between 1700 and 1780 cm^{-1}. The rhodopsin difference spectrum has four prominent bands due to three membrane-embedded carboxylic groups in rhodopsin: two bands at 1770 (−) and 1750 (+) cm^{-1} due to D83 (*52*, *69*), a band at 1728 (−) cm^{-1} and a shoulder at 1745 (+) cm^{-1} due to E122 (*52*) and the ester C═O stretching modes of the phospholipids (*70*), and a band at 1711 cm^{-1} due to E113 (*52*, *71*). In contrast, the VCOP spectrum does not have any detectable bands in this region, which is not surprising in light of the single membrane-embedded carboxylic acid at position 108 (D), equivalent to position 113 in rhodopsin, presumably the counterion. The absence of a counterion band in the region above 1700 cm^{-1} in the VCOP difference spectrum could be due to several reasons. First, the protonated carboxylic acid frequency may be significantly downshifted in VCOP when compared to the rhodopsin carboxylic acid frequencies (>1700 cm^{-1}). Alternatively, the band is present in the region between 1760 and 1700 cm^{-1}, but cannot be observed because it is overlapped by an equally

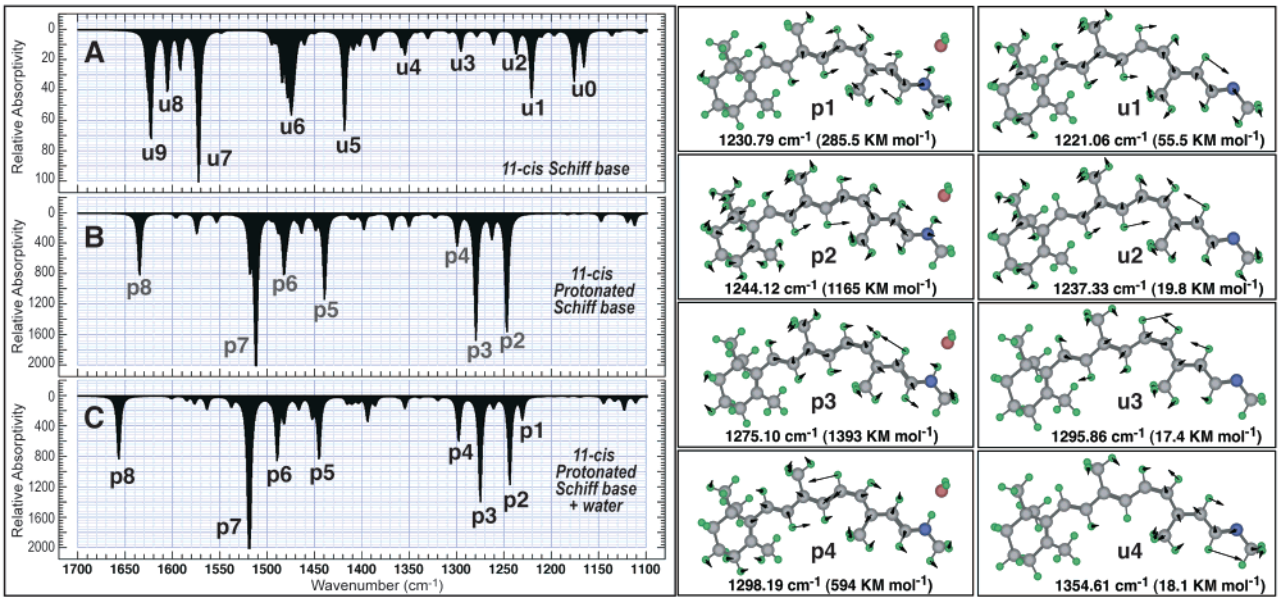

FIGURE 9: Theoretical simulations of the vibrational modes of the Schiff base and protonated Schiff base of 11-*cis*-retinal: Schiff base (A), protonated Schiff base without water (B), and protonated Schiff base with water (C). All calculations were carried out using density functional theory (B3LYP) and a 6-31G basis set. Selected complex C−C stretch and C−H bending modes in the 1200−1400 cm^{-1} region are shown at right, with the mode descriptions and peaks designated using the letters p (protonated) and u (unprotonated). The arrows show the direction of atom motion during a single phase of the vibration, and the length is proportional, but exaggerates, the amount of motion. Additional mode descriptions for the unprotonated chromophore are as follows: u0 (pair of modes involving C_{13}═C_{14}−C_{15} bending mixed with C−H bending modes nearby), u5 and u6 (C−H bends primarily involving the polyene chain methyl groups), u7 (coupled C═C mode involving primarily C_7═C_8, C_9═C_{10}, C_{11}═C_{12}, and C_{13}═C_{14}), u8 (coupled C═C mode involving C_5═C_6, C_7═C_8, C_{11}═C_{12}, C_{13}═C_{14}, and C_{15}═N), and u9 (lysine mode not properly described in this simulation). Additional mode descriptions for the protonated chromophore are as follows: p5 and p6 (C−H bends involving polyene Hs and polyene methyl groups), p7 [very intense (2617 KM/mol) coupled C═C mode involving C_5═C_6, C_7═C_8, C_{11}═C_{12}, and C_{13}═C_{14}], and p8 (imine N−H bending mode coupled with the C_{11}═C_{12} stretch and the C_{14}−C_{15}═N in-plane bend).

intense negative band, and thus canceled out. We also considered the possibility that the *meta II* intermediate was not trapped in these experiments, but we discounted this possibility on the basis of the observation of the *meta II* intermediate at 263 K in the temperature trapping experiments (Figure 5, and previous discussion).

In summary, the C−C stretching band of the chromophore provides the strongest evidence for a protonated Schiff base in VCOP. The vibrational modes that contribute to the composite band between 1240 and 1230 cm^{-1} have not been thoroughly studied in the literature, although there is consensus that these bands are due to C−C modes coupled to hydrogen in-plane bends (see the discussion above). We have carried out a series of ab initio molecular orbital calculations on model 11-*cis* chromophores. There are a number of calculated vibrations in the region from 1200 to 1500 cm^{-1} (Figure 9). The strong vibration in the 1230−1240 cm^{-1} region of the visual pigments seems to be described well using a simple theoretical model based on an 11-*cis* protonated Schiff base (PSB) mediated by a single perchlorate counterion (Figure 10). The significant intensity of this mode in the PSB compounds can be traced to the large variation in atomic charges along the chromophore, which generates a large change in dipole moment during the vibrational motion. In the unprotonated SB, the charge distribution is much less varied and the intensity of the comparable mode is at least an order of magnitude smaller (Figure 9). What remains to be explained is why only one vibration appears in this region while three or four are predicted with comparable intensity. We suggest that conformational distortion of the chromophore within the binding site broadens some of the vibrational bands in this region. The integral of the vibrational distribution suggests that there are other bands in this region, but few survive as sharp lines due to inhomogeneous broadening of the environment.

To do a quantitative comparison of the theoretical and experimental results, we normalized the difference spectra by reference to the absolute intensity of the parent amide I band at ~1650 cm^{-1}. We integrated under the light minus dark spectra of rhodopsin, E113Q (pH 8.2), and violet cone opsin from 1500 to 1100 cm^{-1} (see Table 1). All the values in Table 1 are negative because the dark state, in each case, has greater absorptivity in this region than the light (*meta II*) state. The integral values of rhodopsin and VCOP are similar in magnitude and much larger than the value of the unprotonated E113Q mutant. We suggest that this integral provides the single best determinant of protonation state. We conclude that the chromophore in VCOP is protonated in the dark and becomes deprotonated in the *meta II* intermediate.

Wavelength Regulation in Rhodopsin and the Violet Cone Opsin

We explore in this section the molecular origins of wavelength regulation in both rhodopsin and VCOP. We briefly examine the nature of wavelength regulation in rhodopsin, prior to a re-examination of the role of the counterion position in mediating spectral tuning, considered in our previous work (*14*) on the violet opsin.

Rhodopsin. The rhodopsin crystal structure indicates three glutamic acid residues in the proximity of the chromophore (E122, E181, and E113) as well as a histidine residue (H211)

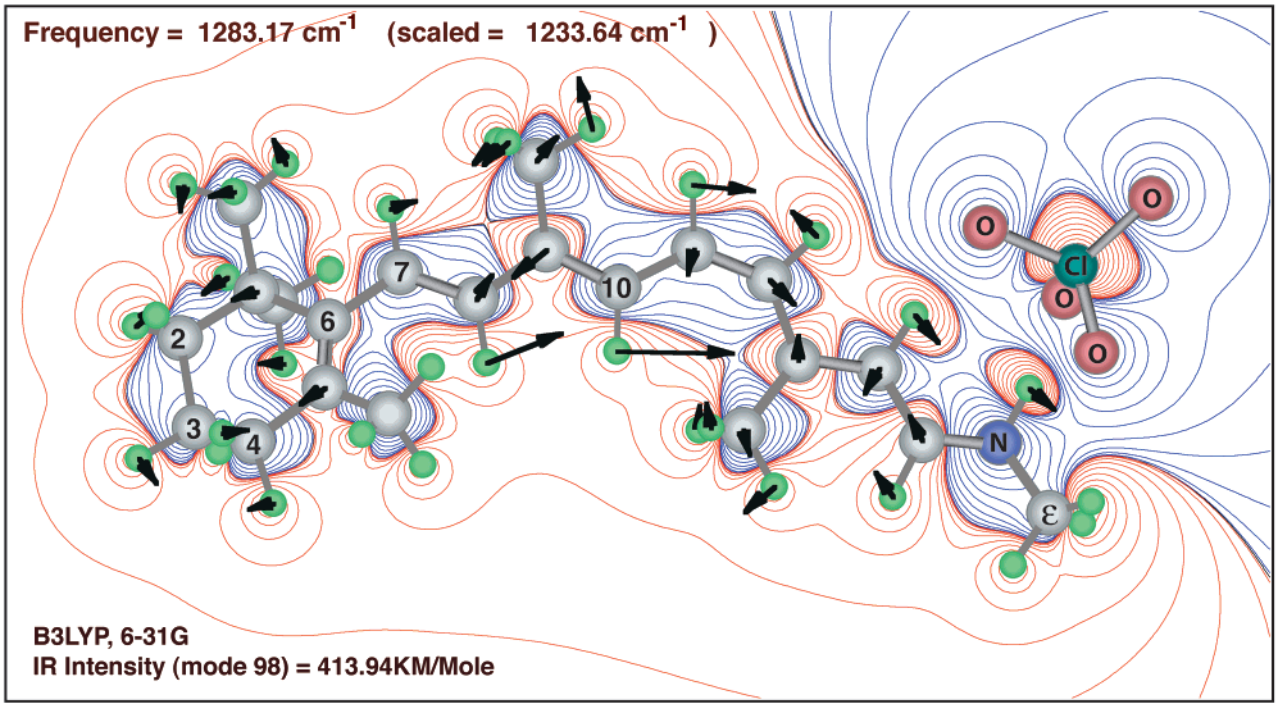

FIGURE 10: Vibrational mode (1232 cm^{-1}) observed in VCOP described well using a simple theoretical model based on an 11-*cis* protonated Schiff base mediated by a single perchlorate counterion. The above mode description was calculated by using DFT molecular orbital theory (B3LYP, 6-31G) (*39*), and the vibrational frequency was scaled by using the appropriate scaling factor of Scott and Radom (*79*). The atomic motion during the vibration generates a large change in dipole moment, visualized above using electrostatic field contours (red being positive and blue negative). This vibration corresponds to mode p2 shown in Figure 9. Note that the mode arrows cross many contour lines, in contrast to a comparable map drawn for the corresponding unprotonated Schiff base mode (u2, Figure 9, electrostatic contours not shown).

near the β-ionylidene ring (*72*). The crystal structure indicates that E122 and H211 are sufficiently close to form a salt bridge. Simple pK_a calculations on the binding site clearly indicate that E113 is deprotonated, but the results are inconclusive on the status of E122 and H211, which are predicted to either be both charged [E122(−)...H211(+)] or both neutral (E122, H211). Previous UV−vis and FTIR studies have concluded that E122 is protonated (*52*, *73*, *74*). However, the evidence is not conclusive because an interaction of E122(−) with H211(+) might produce vibrational and electronic signatures similar to protonation, and the small shifts observed upon replacement of E122 with uncharged residues could be due to a simultaneous deprotonation of H211. The pK_a calculations were also inconclusive regarding the protonation state of E181. If we assume E181 is protonated, then the binding site is neutral, in agreement with the two-photon studies (*75*). To explore all possibilities, however, we assumed that all four residues were charged in the simulations below.

The principal residues within the binding site are shown in Figure 11A together with the participation of individual residues in wavelength regulation based on the use of MNDO-PSDCI molecular orbital theory (*40*, *47*). The isolated 11-*cis*, 6-s-*cis* chromophore is calculated to have an absorption maximum at 588 nm (2.107 eV), while in rhodopsin, the actual absorption maximum is blue-shifted by ~0.38 eV. Calculations were first performed to determine the effect of individual residues on the absorption properties of a protonated Schiff base chromophore, maintaining the geometry of the rhodopsin crystal structure. The energy shifts for each individual residue are shown in electronvolts (eV) in Figure 11A. If the individual contributions (ignoring that of water) are added, a net blue shift of 0.06 is found, far smaller than the observed value. Even if one water molecule hydrogen bonded to the Schiff base proton is included, the additional blue shift of 0.16 only yields a net shift of 0.22, which is still too small. However, when an MNDO-PSDCI calculation is carried out, including the entire first shell of the binding site plus water, a blue shift of 0.43 and an absorption maximum of 488 nm are found. This value is in much better agreement with experiment, and suggests that wavelength mediation in rhodopsin is due in part to second-order interactions not adequately described by simple sum rules based on individual residue shifts. The type of secondary interactions relevant to this process include dipole−dipole and dipole−induced dipole interactions that produce subtle changes in the orientation of polar groups, alter, or enhance the dipole moment vector of a residue, and in combination change the effective reaction field of the binding site.

We note also that E181 is very near the electrostatic null point in the binding site (see Figure 9 of ref *14*). Thus, this residue contributes very little to the wavelength regulation process regardless of ionization state. This observation is in general agreement with site-directed mutagenesis studies of rhodopsin by Nathans (*76*, *77*) and Terakita et al. (*78*). These investigators found either no effect (*76*, *77*) or a small red shift [10 nm (*78*)] (our calculations predict a 0.02 eV or 4 nm red shift). However, the corresponding glutamic acid residue in retinochrome, a photoisomerase in squid photoreceptor cells, is found to provide the primary counterion (retinochrome lacks the glutamic acid residue at position 113) (*78*). We note that our calculations are extremely sensitive to the location of this residue, and a small 1 Å shift toward

Table 1: Comparison of Observed and Calculated Integrals for the *Meta II* Minus Dark FTIR Difference Spectra[a]

Experimental			
protein	pH	Schiff base	integral value
solubilized rhodopsin	6.8	protonated	−0.149 ± 0.037
E113Q rhodopsin	8.2	unprotonated	−0.034 ± 0.042
VCOP	6.8	see the Discussion	−0.146 ± 0.051

Theoretical			
11-*cis* chromophore	method[b]	p2 band (intensity)[c]	integral value
unprotonated Schiff base (SB)	B3LYP, 6-31G	1221.1 (55.5)	−0.014
SB	B3LYP, 6-31G(d)	1203.8 (63.2)	0.006
protonated Schiff base (PSB)	B3LYP, 6-31G	1247.2 (1579.5)	−0.816
PSB[d]	B3LYP, 6-31G(d)	1224.3 (1966.3)	−0.827
PSB with water	B3LYP, 6-31G	1244.1 (1165.2)	−0.745
PSB with perchlorate[e]	B3LYP, 6-31G	1233.6 (413.9)	−0.262
PSB with perchlorate in water[f]	B3LYP, 6-31G	1237.8 (1117.6)	−0.744
PSB with perchlorate and two waters	HF, 6-31G	1239.7 (450.3)	−0.206
PSB with perchlorate and two waters	HF, 6-31G(d)	1218.9 (443.0)	−0.180

[a] All the experimental integral values are for the *meta II* intermediate minus the dark state and were measured from 1100 to 1500 cm^{-1} in units of cm^{-1} with the values normalized by adjusting the amide I band absorptivity to 1. The theoretical values are calculated relative to the all-*trans* unprotonated Schiff base (e.g., *meta II*-like) chromophore (B3LYP, 6-31G) with the integrals normalized to the central amide I band of polyglycine multiplied by the total number of residues in the protein (see the Discussion). [b] Calculations were carried out using *Gaussian 98* (*39*). [c] Location in wavenumber of the intense mode, labeled p2 in the isolated protonated Schiff base, which corresponds to the observed mode at ∼1238 cm^{-1} in rhodopsin and by analogy at 1232 cm^{-1} in VCOP. The intensity is in KM/mol. [d] The results of the B3LYP 6-31G(d) (e.g., 6-31G*) calculation are similar to those shown in Figure 9B, but the peak labeled p2 is now the strongest peak in the spectrum. The single water molecule is hydrogen bonded to the Schiff base proton (see Figure 9). [e] Molecule and vibration shown in Figure 10. [f] The solvent environment was simulated by using a spherical Onsager reaction field and carrying out the minimization using a dielectric constant of 78 and a cavity radius of 10 Å.

the imine linkage transforms a small red shift to a large (30 nm) blue shift.

Violet Cone Opsin. We examined the violet cone opsin binding site on the basis of a similarity replacement of the rhodopsin side chains with the corresponding residues of violet cone opsin. The rhodopsin backbone was held fixed during the process, and an energy minimization was carried out after the replacement residues were inserted. The results are shown in Figure 11B. The N-terminal end of VCOP is shorter by five residues than rhodopsin, and one must add 5 to the residue numbers in Figure 11B to find the corresponding rhodopsin residue in Figure 11A (for example, D108 in VCOP correlates with E113 in rhodopsin).

We have not carried out calculations for the individual shifts for each binding site residue in VCOP, because our calculations on rhodopsin indicate that individual residue shifts are not additive (see above). VCOP has an absorption maximum at 425 nm (2.915 eV), which represents a blue shift of 0.43 eV relative to that of rhodopsin. A comparison of panels A and B of Figure 11 suggests that the single largest change in going from the rhodopsin to the VCOP binding site is the loss of the E122-H211 pair near the β-ionylidene ring. As shown in Figure 11A, this charged pair provides a

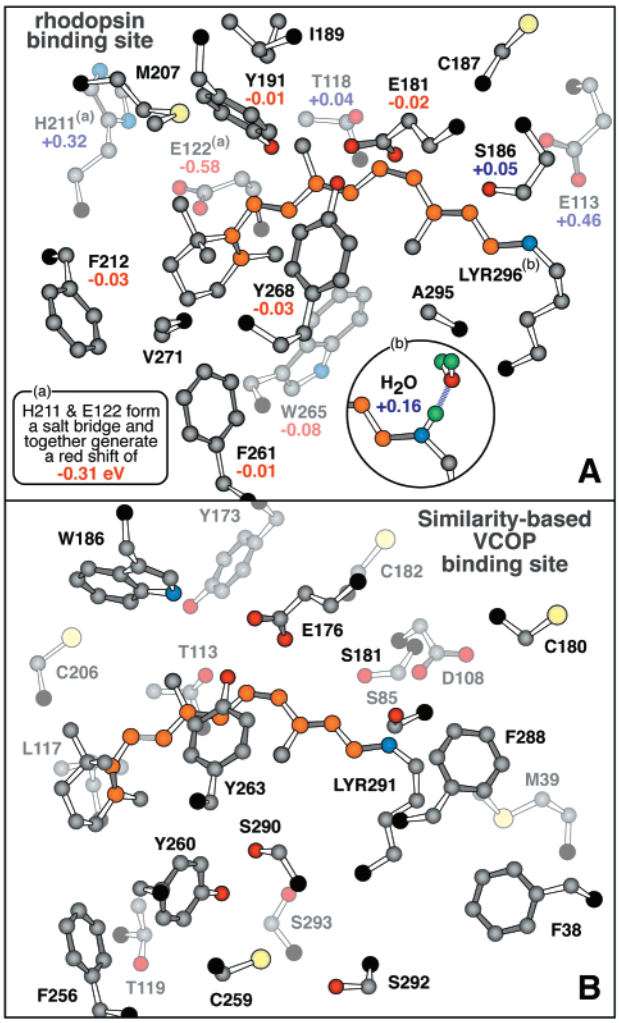

FIGURE 11: Rhodopsin and violet cone opsin chromophore binding sites. A comparison of the rhodopsin binding site (A) and a similarity-based preliminary model of the VCOP binding site (B). The coordinates for the rhodopsin binding site are from the crystal structure, but the water molecule near the Schiff base was added and minimized by us. The VCOP model was generated using a similarity transformation (see the text). First-order λ_{max} band transition energy shifts associated with nearby residues in rhodopsin were calculated using MNDO-PSDCI molecular orbital theory and are indicated in electronvolts under the residue name in panel A. Negative numbers represent red shifts, and positive numbers represent blue shifts. The shift for each residue is based on that residue and the chromophore alone, and all other residues are ignored unless noted. The shifts calculated for the Glu and His residues assume a nominally charged [Glu(−), His(+)] residue. Most experimental studies of rhodopsin conclude that LYR296 is positively charged, E113 is negatively charged, and all other residues shown in panel A are uncharged (see the Discussion).

first-order red shift of −0.31 eV, and by itself would account for ∼75% of the blue shift required. The E122-H211 pair is also absent from the human blue cone. As noted above, the results of some site-directed mutagenesis studies on E122 have been interpreted to indicate that this residue is protonated in rhodopsin (*52*, *73*, *74*). However, strong interaction with H211 could produce vibrational and electronic signatures that are similar to direct protonation, and further work on the characterization of the protonation state of E122 would be welcome.

An MNDO-PSDCI calculation on the first shell of the VCOP binding site model shown in Figure 11B predicts an

absorption maximum at 433 nm. The calculated blue shift of 0.32 eV is in respectable agreement with the observed rhodopsin to VCOP blue shift of 0.43 eV. We conclude that our simple binding site analysis is correct to first order, and provides a realistic perspective on the primary components of wavelength regulation in VCOP.

It is likely that any model of wavelength regulation which relies solely on the location and charges of a few individual residues will fail to have global applicability. We suggest that a significant portion of wavelength regulation is accomplished via evolution of the entire binding site ensemble involving 10−20 residues and that secondary interactions among these residues provide the dominant electrostatic and dispersive wavelength shifts.

SUMMARY AND CONCLUSIONS

We show that the *Xenopus* violet cone opsin has a protonated Schiff base chromophore in the dark, and undergoes a series of conformational changes upon excitation that can be identified as the *batho*, *lumi*, *meta I*, and *meta II* photoproducts. The absorption spectra of these intermediates have been recorded, and the photobleaching sequence is quite similar to that observed in rhodopsin, but blue shifted. When these two systems are compared on the basis of wavelength mediation along the photobleaching pathway, the similarities are striking (Figure 7). Like that of rhodopsin and the other visual pigments, light activation of the *Xenopus* violet cone opsin initiates a sequence of events that leads to the formation of the biologically active state, *meta II*, and the ultimate expulsion of the chromophore from the binding pocket.

A similarity transformation of the rhodopsin binding site generates a model for the VCOP binding site that predicts roughly 75% of the observed blue shift of the violet cone relative to rhodopsin. The MNDO-PSDCI calculations indicate that secondary interactions between the binding site residues are just as important as first-order chromophore protein interactions at the mediating wavelength. The importance of secondary interactions in wavelength regulation complicates and may even preclude assignment of a simple mechanism for wavelength regulation that applies to all pigments. An example of such a mechanism would be one based on the strategic placement of a single negatively charged residue as we proposed earlier (*14*). Evolution of the entire pocket rather than adjustment of a single charged residues is not an unexpected consequence. Evolution of a visual pigment must optimize simultaneously (1) the wavelength maximum, (2) the quantum efficiency for the primary photochemical event, and (3) energy storage to drive the photobleaching thermal reactions and conformational processes responsible for activation. Strategic placement of a single residue cannot accomplish all three goals simultaneously.

The observation of a significantly red-shifted photoproduct in VCOP, only observed upon extended illumination, remains a unique and not fully understood aspect of the VCOP primary photochemical event. We suggest that this red-shifted state is due to relaxation of the chromophore into a more planar conformation via a pathway normally blocked by one or more residues in the binding site. Repeated photochemical transformation of the chromophore rearranges the local protein environment and causes the blocking residues to shift to higher-energy conformations that accommodate a more planar all-*trans* chromophore. The presence of this intermediate, not relevant to the primary photobleaching sequence, suggests that the binding site of VCOP is more compact than rhodopsin and a majority of the other visual pigments.

ACKNOWLEDGMENT

We thank Prof. Jerry Goodisman for interesting and helpful discussions, and the National Science Foundation for generous allocations of supercomputer time at the San Diego and Illinois supercomputer facilities.

REFERENCES

1. Schnapf, J., and Baylor, D. A. (1986) *Sci. Am. 256*, 32−39.
2. Yau, K. W. (1994) *Invest. Ophthalmol. Visual Sci. 35*, 9−32.
3. Baylor, D. (1996) *Proc. Natl. Acad. Sci. U.S.A. 93*, 560−565.
4. Wald, G. (1968) *Nature 219*, 800−808.
5. Oseroff, A. R., and Callender, R. H. (1974) *Biochemistry 13*, 4243−4348.
6. Hargrave, P. A., Mcdowell, J. H., Curtis, D. R., Wang, J. K., Juszczak, E., Fong, S. L., Rao, J. K. M., and Argos, R. (1983) *Biophys. Struct. Mech. 9*, 235−244.
7. Hargrave, P. A., and McDowell, J. H. (1992) *FASEB J. 6*, 2323−2331.
8. Scott, K., Becker, A., Sun, Y., Hardy, R., and Zuker, C. (1995) *Neuron 15*, 919−927.
9. Okano, T., Kojima, D., Fukada, Y., Shichida, Y., and Yoshizawa, T. (1992) *Proc. Natl. Acad. Sci. U.S.A. 89*, 5932−5936.
10. Yoshizawa, T. (1994) *Biophys. Chem. 50*, 17−24.
11. Yokoyama, S. (1995) *Mol. Biol. Evol. 12*, 53−61.
12. Yokoyama, S., Radlwimmer, F., and Blow, N. (2000) *Proc. Natl. Acad. Sci. U.S.A. 97*, 7366−7371.
13. Ebrey, T., and Koutalos, Y. (2001) *Prog. Retinal Eye Res. 20*, 49−94.
14. Vought, B. W., Dukkipatti, A., Max, M., Knox, B. E., and Birge, R. R. (1999) *Biochemistry 38*, 11287−11297.
15. Jacobs, G. H., Deegan, G. F., and Neitz, J. (1998) *Vision Neurol. 15*, 581−584.
16. Merbs, S., and Nathans, J. (1992) *Nature 356*, 443−435.
17. Okano, T., Fukada, Y., Artamonov, I. D., and Yoshizawa, T. (1989) *Biochemistry 28*, 8848−8856.
18. Kawamura, S., and Yokoyama, S. (1997) *Vision Res. 38*, 37−44.
19. Yokoyama, S., Radlwimmer, F. B., and Kawamura, S. (1998) *FEBS Lett. 423*, 155−158.
20. Hisatomi, O., Satoh, T., Barthel, L. K., Stenkamp, D. L., Raymond, P. A., and Tokunga, F. (1996) *Vision Res. 36*, 933−939.
21. Kliger, D. S., and Lewis, J. W. (1995) *Isr. Jour. Chem. 35*, 289−307.
22. Yoshizawa, T., and Shichida, Y. (1982) in *Methods in Enzymology*, pp 333−354, Academic Press, New York.
23. Yoshizawa, T., and Wald, G. (1967) *Nature 214*, 566−571.
24. Shichida, Y., Imai, H., Imamoto, Y., Fukada, Y., and Yoshizawa, T. (1994) *Biochemistry 33*, 9040−9044.
25. Tsuda, M., Tokunga, F., Ebrey, T. G., Yue, K. T., Marque, J., and Eisenstein, L. (1980) *Nature 287*, 461−462.
26. Imai, H., Imamoto, Y., Yoshizawa, T., and Shichida, Y. (1995) *Biochemistry 34*, 10525−10531.
27. Kojima, D., Imai, H., Okano, T., Fukada, Y., Crescitelli, F., Yoshizawa, T., and Shichida, Y. (1995) *Biochemistry 34*, 1096−1106.
28. Archer, S., and Hirano, J. (1996) *Proc. R. Soc. London, Ser. B 263*, 761−767.
29. Baldwin, P., and Hubbell, W. (1993) *EMBO J. 12*, 1693−1703.
30. Lin, S. W., Kochendoerfer, G. G., Caroll, K. S., Wang, D., Mathies, R. A., and Sakmar, T. P. (1998) *J. Biol. Chem. 273*, 24583−24591.

31. Kochendoerfer, G. G., Wang, Z., Oprian, D. D., and Mathies, R. A. (1997) *Biochemistry 36*, 6577−6587.
32. Wilkie, S. E., Vissers, P. M. A. M., Das, D., DeGrip, W. J., Bowmaker, J. K., and Hunt, D. M. (1998) *Biochem. J. 330*, 541−547.
33. Chang, B. S. W., Crandall, K. A., Carulli, J. P., and Hartl, D. L. (1995) *Mol. Phylogenet. Evol. 4*, 31−43.
34. Yokoyama, S., and Zhang, H. (1997) *Gene 202*, 89−93.
35. Starace, D. M., and Knox, B. E. (1997) *J. Biol. Chem. 272*, 1095−1100.
36. Starace, D. M., and Knox, B. E. (1998) *Exp. Eye Res. 67*, 209−220.
37. Sakmar, T. P., Franke, R. R., and Khorana, H. G. (1989) *Proc. Natl. Acad. Sci. U.S.A. 86*, 8309−8313.
38. De Grip, W. J. (1982) in *Methods in Enzymology* (Packer, L., Ed.) pp 197−207, Academic Press, New York.
39. Frisch, M. J., Trucks, G. W., Schlegel, H. B., Scuseria, G. E., Robb, M. A., Cheeseman, J. R., Zakrzewski, V. G., Montgomery, J. A., Stratmann, R. E., Burant, J. C., Dapprich, S., Millam, J. M., Daniels, A. D., Kudin, K. N., Strain, M. C., Farkas, O., Tomasi, J., Barone, V., Cossi, M., Cammi, R., Mennucci, B., Pomelli, C., Adamo, C., Clifford, S., Ochterski, J., Petersson, G. A., Ayala, P. Y., Cui, Q., Morokuma, K., Malick, D. K., Rabuck, A. D., Raghavachari, K., Foresman, J. B., Cioslowski, J., Ortiz, J. V., Stefanov, B. B., Liu, G., Liashenko, A., Piskorz, P., Komaromi, I., Gomperts, R., Martin, R. L., Fox, D. J., Keith, T., Al-Laham, M. A., Peng, C. Y., Nanayakkara, A., Gonzalez, C., Challacombe, M., Gill, P. M. W., Johnson, B. G., Chen, W., Wong, M. W., Andres, J. L., Head-Gordon, M., Replogle, E. S., and Pople, J. A. (1998) *Gaussian 98*, Gaussian Inc., Pittsburgh, PA.
40. Martin, C. H., and Birge, R. R. (1998) *J. Phys. Chem. A 102*, 852−860.
41. Barlow, R. B., Birge, R. R., Kaplan, E., and Tallent, J. R. (1993) *Nature 366*, 64−66.
42. Stuart, J. A., Vought, B. W., Zhang, C. F., and Birge, R. R. (1995) *Biospectroscopy 1*, 9−28.
43. Yamazaki, M., Goodisman, J., and Birge, R. R. (1998) *J. Chem. Phys. 108*, 5876−5887.
44. Birge, R. R., Zgierski, M. Z., Serrano-Andres, L., and Hudson, B. S. (1999) *J. Phys. Chem. A 103*, 2251−2255.
45. Birge, R. R., Gillespie, N. B., Izaguirre, E. W., Kusnetzow, A., Lawrence, A. F., Singh, D., Song, Q. W., Schmidt, E., Stuart, J. A., Seetharaman, S., and Wise, K. J. (1999) *J. Phys. Chem. B. 103*, 10746−10766.
46. Hudson, B. S., and Birge, R. R. (1999) *J. Phys. Chem. 103*, 2274−2281.
47. Kusnetzow, A., Singh, D. L., Martin, C. H., Barani, I., and Birge, R. R. (1999) *Biophys. J. 76*, 2370−2389.
48. Tachibanaki, S., Imamoto, Y., Imai, H., and Shichida, Y. (1995) *Biochemistry 34*, 13170−13175.
49. Imamoto, Y., Yoshizawa, T., and Shichida, Y. (1996) *Biochemistry 35*, 14599−14607.
50. Imamoto, Y., Yoshizawa, T., and Shichida, Y. (1996) *Biochemistry 35*, 14599−14607.
51. Jäger, F., Fahmy, K., Sakmar, T. P., and Siebert, F. (1994) *Biochemistry 33*, 10878−10882.
52. Fahmy, K., Jaeger, F., Beck, M., Zvyaga, T. A., Sakmar, T. P., and Siebert, F. (1993) *Proc. Natl. Acad. Sci. U.S.A. 90*, 10206−10210.
53. Zvyaga, T., Fahmy, K., Siebert, F., and Sakmar, T. (1996) *Biochemistry 35*, 7536−7545.
54. Fahmy, K., Sakmar, T., and Siebert, F. (2000) *Methods Enzymol. 315*, 178−196.
55. Callender, R. H., and Honig, B. (1977) *Annu. Rev. Biophys. Bioeng. 6*, 33−55.
56. Siebert, F. (1995) *Isr. J. Chem. 35*, 309−323.
57. Hug, S. J., Lewis, J. W., Einterz, C. M., Thorgeirsson, T. E., and Kliger, D. S. (1990) *Biochemistry 29*, 1475−1485.
58. Kito, Y., Suzuki, T., Azuma, M., and Sekoguti, Y. (1968) *Nature 218*, 955−957.
59. Longstaff, C., Calhoon, R. D., and Rando, R. R. (1986) *Proc. Natl. Acad. Sci. U.S.A. 83*, 4209−4213.
60. Mathies, R., Freedman, T. B., and Stryer, L. (1977) *J. Mol. Biol. 109*, 367−372.
61. Doukas, A. G., Aton, B., Callender, H., and Ebrey, T. G. (1978) *Biochemistry 17*, 2430−2435.
62. Ganter, U. M., Gärtner, W., and Siebert, F. (1988) *Biochemistry 27*, 7480−7488.
63. Ganter, U., Schmid, E., and Siebert, F. (1988) *J. Photochem. Photobiol., B 2*, 417−426.
64. Palings, J., Pardoen, J. A., van der Berg, E., Winkel, C., Lugtenburg, J., and Mathies, R. S. (1987) *Biochemistry 26*, 2544−2556.
65. Siebert, F., and Mäntele, W. (1980) *Biophys. Struct. Mech. 6*, 147−164.
66. Fahmy, K., Weidlich, O., Engelhard, M., Tittor, J., Oesterhelt, D., and Siebert, F. (1992) *Photochem. Photobiol. 56*, 1073−1083.
67. Fahmy, K., Siebert, F., and Sakmar, T. P. (1994) *Biochemistry 33*, 13700−13705.
68. Nakanishi, K., and Crouch, R. (1995) *Isr. J. Chem. 35*, 253−272.
69. Rath, P., DeCaluwe, L. L. J., Bovee-Geurts, P. H. M., DeGrip, W. J., and Rothschild, K. J. (1993) *Biochemistry 32*, 10277−10282.
70. Beck, M., Siebert, F., and Sakmar, T. (1998) *FEBS Lett. 436*, 304−308.
71. Jäger, F., Jäger, S., Kräutle, O., Friedman, N., Sheves, M., Hofmann, K., and Siebert, F. (1994) *Biochemistry 33*, 7389−7397.
72. Palczewski, K., Kumasaka, T., Hori, T., Behnke, C. A., Motoshima, H., Fox, B. A., Le Trong, I., Teller, D. C., Okada, T., Stenkamp, R. E., Yamamoto, M., and Miyano, M. (2000) *Science 289*, 739−745.
73. DeCaluwe, G. L. J., Bovee-Geurts, P. H. M., Rath, P., Rothschild, K. J., and de Grip, W. J. (1995) *Biophys. Chem. 56*, 79−87.
74. Nagata, T., Terakita, A., Kandori, H., Shichida, Y., and Maeda, A. (1998) *Biochemistry 37*, 17216−17222.
75. Birge, R. R., Murray, L. P., Pierce, B. M., Akita, H., Balogh-Nair, V., Findsen, L. A., and Nakanishi, K. (1985) *Proc. Natl. Acad. Sci. U.S.A. 82*, 4117−4121.
76. Nathans, J. (1990) *Biochemistry 29*, 937−942.
77. Nathans, J. (1990) *Biochemistry 29*, 9746−9752.
78. Terakita, A., Yamashita, T., and Shichida, Y. (2000) *Proc. Natl. Acad. Sci. U.S.A. 97*, 14263−14267.
79. Scott, A. P., and Radom, L. (1996) *J. Phys. Chem. 100*, 16502−16513.

BI010387Y